Thoracic Cancer

Open Access

Thoracic Cancer ISSN 1759-7706

ORIGINAL ARTICLE

# Prediction of tumor doubling time of lung adenocarcinoma using radiomic margin characteristics

Hyun Jung Yoon[1,2†], Hyunjin Park[3,4†], Ho Yun Lee[1,5], Insuk Sohn[6], Joonghyun Ahn[6] & Seung-Hak Lee[7]

1 Department of Radiology and Center for Imaging Science, Samsung Medical Center, Sungkyunkwan University School of Medicine, Seoul, South Korea
2 Department of Radiology, Veterans Health Service Medical Center, Seoul, South Korea
3 School of Electronic and Electrical Engineering, Sungkyunkwan University, Suwon, South Korea
4 Center for Neuroscience Imaging Research, Institute for Basic Science, Suwon, South Korea
5 Department of Health Sciences and Technology, SAIHST, Sungkyunkwan University, Seoul, South Korea
6 Statistics and Data Center, Samsung Medical Center, Seoul, South Korea
7 Department of Electrical and Computer Engineering, Sungkyunkwan University, Suwon, South Korea

**Keywords**
Computed tomography; lung adenocarcinoma; radiomics; tumor doubling time; tumor margin.

**Correspondence**
Ho Yun Lee, Department of Radiology and Center for Imaging Science, Samsung Medical Center, Sungkyunkwan University School of Medicine, 81 Irwon-Ro, Gangnam-Gu, Seoul 06351, South Korea; and Department of Health Sciences and Technology, SAIHST, Sungkyunkwan University, Seoul 06351, South Korea.
Tel: +82 2 3410 2502
Fax: +82 2 3410 0049
Email: hoyunlee96@gmail.com

†These authors contributed equally to this work.

Received: 24 May 2020;
Accepted: 30 June 2020.

doi: 10.1111/1759-7714.13580

Thoracic Cancer **11** (2020) 2600–2609

## Abstract

**Background:** Because shape or irregularity along the tumor perimeter can result from interactions between the tumor and the surrounding parenchyma, there could be a difference in tumor growth rate according to tumor margin or shape. However, no attempt has been made to evaluate the correlation between margin or shape features and tumor growth.

**Methods:** We evaluated 52 lung adenocarcinoma (ADC) patients who had at least two computed tomographic (CT) examinations before curative resection. Volume-based doubling times (DTs) were calculated based on CT scans, and patients were divided into two groups according to the growth pattern (GP) of their ADCs (gradually growing tumors [GP I] vs. growing tumors with a temporary decrease in DT [GP II]). CT radiomic features reflecting margin characteristics were extracted, and radiomic features reflective of tumor DT were selected.

**Results:** Among the 52 patients, 41 (78.8%) were assigned to GP I and 11 (21.2%) to GP II. Of the 94 radiomic features extracted, eccentricity, surface-to-volume ratio, LoG uniformity ($\sigma$ = 3.5), and LoG skewness ($\sigma$ = 0.5) were ultimately selected for tumor DT prediction. Selected radiomic features in GP I were surface-to-volume ratio, contrast, LoG uniformity ($\sigma$ = 3.5), and LoG skewness ($\sigma$ = 0.5), similar to those for total subjects, whereas the radiomic features in GP II were solidity, energy, and busyness.

**Conclusions:** This study demonstrated the potential of margin-related radiomic features to predict tumor DT in lung ADCs.

## Key points

**Significant findings of the study:** We found a relationship between margin-related radiomic features and tumor doubling time.

**What this study adds:** Margin-related radiomic features can potentially be used as noninvasive biomarkers to predict tumor doubling time in lung adenocarcinoma and inform treatment strategies.

## Introduction

Sequential computed tomography (CT) scans and pulmonary tumor volume measurements are useful for assessing tumor growth rates.[1] On sequential CT scan images, it is important to determine whether a pulmonary nodule has grown and, if it has, how fast it has grown. The doubling

 © 2020 The Authors. *Thoracic Cancer* published by China Lung Oncology Group and John Wiley & Sons Australia, Ltd. This is an open access article under the terms of the Creative Commons Attribution-NonCommercial-NoDerivs License, which permits use and distribution in any medium, provided the original work is properly cited, the use is non-commercial and no modifications or adaptations are made.

time (DT) of pulmonary tumors, which is the mean time for a tumor to double in volume, is used to differentiate malignant from benign tumors.[2, 3] In lung cancer in particular, DT reflects tumor cell proliferation and serves as a determinant of tumor aggressiveness.[4] Moreover, the DT of lung cancer on serial CT scans reflects tumor histology and is closely associated with prognosis.[5–8] Thus, the DT of lung cancer is one of the key parameters that is used to distinguish aggressive tumors from indolent ones.

Several studies have investigated the correlation between tumor DT in lung cancer patients and imaging features.[6–10] –10 Solid components of lung cancers on CT images reflect their invasive potential and are associated with rapid growth, whereas ground glass opacity (GGO) components suggest a longer DT and good outcome, such as seen for adenocarcinoma in situ (AIS) and minimally invasive adenocarcinoma (MIA). However, these previous studies only evaluated a few qualitative imaging characteristics, such as solidity.

Radiomics extracts accurate quantitative imaging descriptors from images using image processing techniques,[11] and several studies have attempted to provide descriptive and predictive models relating image features to tumor phenotypes.[12, 13] The majority of features used in classification has been derived from intratumoral descriptors. Peritumoral radiomic features for both disease diagnosis and prognosis of brain, breast, and lung cancers have also been explored.[14–17] In the context of lung cancers, a few studies have indicated that radiomic features of the tumor surroundings can be used to discriminate granulomas from adenocarcinomas (ADCs).[15, 18] Because shape or irregularity along the tumor perimeter can result from interactions between the tumor and the surrounding parenchyma, there could be a difference in tumor growth rate according to tumor margin or shape. To the best of our knowledge, no attempt has been made to evaluate the correlation between margin or shape features and tumor growth, even though these characteristics, which can be extracted from lung CT images, may reflect the tumor microenvironment.

Accordingly, we conducted a study to identify CT imaging features with a focus on margin characteristics that would allow us to predict the tumor DT of lung ADC using a radiomics approach. Our main purpose was to explore the potential of margin-related radiomic features to predict tumor DT in patients with lung ADCs.

# Methods

## Patients and data acquisition

First, we retrieved data from 511 consecutive patients with lung ADC who underwent complete resection at our institution from July 2003 to January 2011. Subjects who had at least two preoperative chest CT examinations with a time interval of at least six months between the first and last preoperative CT to allow us to assess differences in tumor sizes were selected for our study. The first CT was regarded as the initial CT, and the last preoperative CT was regarded as the final CT. Finally, 52 subjects with an adequate CT protocol from which we could extract radiomic features at an optimal resolution were included in our study. This retrospective study was approved by the institutional review board of our institution (institutional review board file number 2016-04-135), and the requirement for informed consent to review patient medical records was waived.

Clinical data were collected from electronic medical records at the time of diagnostic work-up. Sex, age, smoking status, Union for International Cancer Control stage, and operation type were recorded. Histologic reports were also retrieved from electronic medical records, with histological classification based on the International Association for the Study of Lung Cancer/American Thoracic Society/European Respiratory Society multidisciplinary classification of lung ADC.[19]

## Imaging acquisition

All helical CT images were obtained with a 64-detector row CT scanner (LightSpeed VCT, GE Healthcare, Waukesha, WI). CT image parameters were as follows: detector collimation, 1.25 or 0.625 mm; field of view, 36 cm; beam pitch, 1.375 to 1.500; beam width, 10 to 20 mm; gantry speed, 0.5 or 0.6 seconds per rotation; 120 kVp; 125 mA; reconstruction interval, 1 to 2.5 mm; and matrix, 512 × 512 mm. Helical acquisitions were reformatted into contiguous 2.5 to 3.5 mm axial sections overlapping by 1 to 1.5 mm on a standard workstation. CT scanning was performed 90s after administration of contrast material (100 mL of iopamidol [Iomeron 300, Bracco, Milan, Italy]) at a rate of 1.5 mL/second using a power injector. This was followed by a 20 $cm^3$ saline flush at a rate of 1.5 mL/second.

## Tumor doubling time calculations

Reconstructed thin-section CT data were transferred to our personal computer–based in-house software program for lesion segmentation. Two readers independently performed manual segmentation of region of interests (ROIs) on axial CT images to generate a volume of interest that included the entire lesion (both GGO and consolidation components). Tumor volume of ROI was computed by multiplying the number of voxels by the unit volume of a voxel. Initial and final tumor volumes referred to the initial

 © 2020 The Authors. *Thoracic Cancer* published by China Lung Oncology Group and John Wiley & Sons Australia, Ltd. 

tumor volume and final tumor volume, respectively. If additional longitudinal CT images were obtained between the initial and last CT scan date, the two readers also performed segmentation of ROIs for those CT scans. Volume doubling time ($DT_{volume}$) of a tumor was obtained using the following equation:

$$DT_{\text{volume}} = (t \cdot \log 2)/[\log(RC_{\text{volume}})]$$

where t was the interval (in days) between two CT scans, and $RC_{volume}$ was the ratio of volume change of the initial and final volumes for each nodule.[20]

## Growth pattern analysis

Two radiologists performed sequential image review and noted a temporary decrease in tumor volume on serial CT scans in 11 (21.2%) tumors with a GGO component. The temporary decrease in tumor volume, which corresponds to a negative DT, is considered to result from alveolar collapse and central fibrosis with tumor progression causing tumor shrinkage.[21, 22] Thus, the radiologists classified tumors into two groups based on their growth pattern (GP) on serial CT images. The one group comprised patients with gradually growing tumors without a temporary decrease in tumor volume through observation on CT (GP I), ($n$ = 41, 78.8%), while the other group comprised patients with growing tumors with a temporary decrease in tumor volume (negative DT) between the initial and final CT scans (GP II), ($n$ = 11, 21.2%) (Fig 1). If opinions differed with regard to growth pattern, consensus was achieved by discussion.

## Radiomic analysis

Radiomic analysis of initial CT images was performed based on shape, local (texture based), filter-based, and fractal model-based features from the manually derived ROI, which was obtained as described for the tumor volume calculation. Shape, filter-based, and fractal model-based features except local features (texture based) were regarded to be margin-related features. Details are provided in Appendix S1 and the categorization of all features is presented in Table S1. A total of 94 CT radiomic features were calculated using the open-source code (PyRadiomics)[23] and in-house code using MATLAB. Features unavailable in PyRadiomics were implemented using the in-house code and there are several published articles which have been used the same software.[24, 25]

## Data management and statistical analyses

Radiomic feature data from initial CT scans were used to establish a predictor of tumor DT. We utilized 94 radiomic features as the input to assess potential associations of these radiomic features with tumor growth rate.

The $P$-values of all 94 radiomic features were calculated using univariate generalized estimating equations (GEEs) for the initial CT and final CT measures. Features with a $P$-value < 0.1 and clinical significance were selected as significant for tumor DT prediction. Next, to remove redundant radiomic information, we chose more significant features among the selected radiomic features and then constructed a prediction model using multiple GEEs with those final selected features. We performed subgroup analysis according to tumor growth pattern in the same way. To compare the prediction models and verify our results, predicted and observed values were analyzed by Spearman's correlation analysis. The Shapiro-Wilk test was used to verify normality of continuous variable. A flow chart showing the development of our tumor DT prediction model based on radiomic features is shown in Fig 2.

We evaluated the stability of various radiomic features by calculating intraclass correlation coefficients (ICCs) as a measure of interobserver reliability. ICC values >0.4, >0.6, >0.8, and >0.9 were regarded as representing moderate, good, very good, and excellent reproducibility, respectively.[26]

Overall survival (OS) and disease-free survival (DFS) were calculated for all patients who underwent curative operations for lung adenocarcinoma.

# Results

Demographic information and tumor characteristics are listed in Table 1. Prior to complete resection, the median CT interval between the first and last scan was 23.5 months (interquartile range [IQR], 12.5 to 53.5 months).

## Reliability and reproducibility of tumor segmentation and feature extraction

ICC values ranged from 0.59 to 1, with mean a value of 0.91, indicating a moderate or high level of agreement. Most radiomic features showed very good or excellent reproducibility, but kurtosis-related filter-based features showed relatively lower levels of agreement (Table S2).

 © 2020 The Authors. *Thoracic Cancer* published by China Lung Oncology Group and John Wiley & Sons Australia, Ltd.

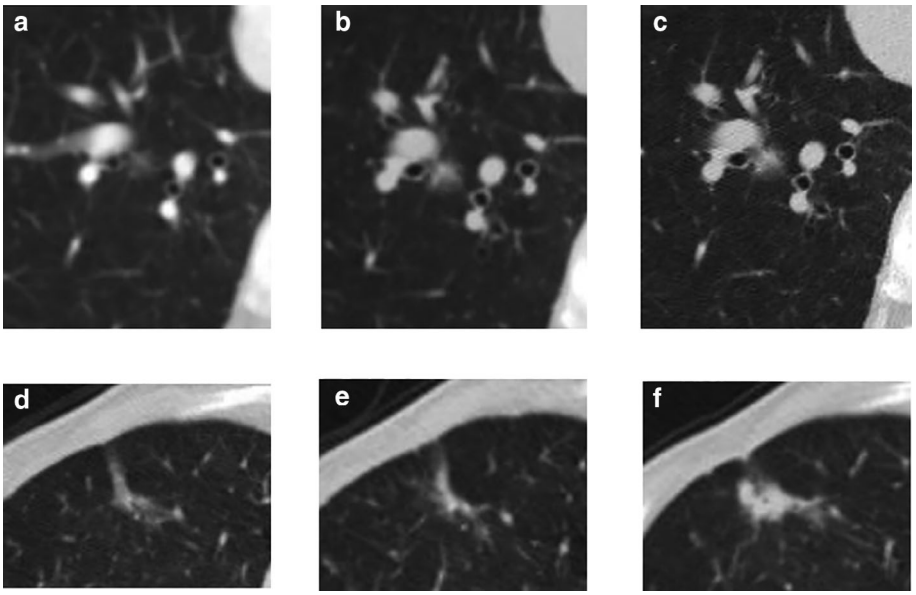


**Figure 1** Serial computed tomographic (CT) images of lung adenocarcinomas according to growth pattern. (**a**–**c**) A case of growth pattern I. (**a**) On the initial CT, a 7 mm pure ground-glass opacity (GGO) nodule was detected in the right lower lobe. (**b**) On follow-up CT after 13 months, a solid component newly appeared in the central area of the GGO. The nodule had increased slightly in size to 9 mm in diameter. (**c**) Six months later, both solid component and GGO area demonstrated an increase in size (11 mm). (**d**–**f**) A case of growth pattern II. (**d**) On the initial CT, an 18 mm part-solid lesion was detected in the right lower lobe. (**e**) One year later, the lesion had decreased in size with a diameter of 14.4 mm. (**f**) After two years, the solid component had become enlarged, while the GGO had decreased.

### Radiomic prediction of tumor doubling time

Of the 94 total features evaluated, 48 with a *P*-value < 0.1 were selected from univariate GEE analysis. Selected radiomic CT image features were eccentricity, surface-to-volume ratio, auto correlation, cluster tendency, variance, busyness, Laplacian of Gaussian (LoG) mean (σ = 0.5–3.5 in 0.5 voxel increments), LoG maximum (σ = 1–3.5), LoG median (σ = 0.5–3.5), LoG entropy (σ = 2–3.5), LoG uniformity (σ = 1.5–3.5), LoG standard deviation (σ = 1.5–3.5), LoG skewness (σ = 0.5), and LoG kurtosis (σ = 0.5–3.5). To remove redundant features, we reduced the list to 30 of the more significant features without redundancy (Table 2). When we performed multiple GEE analyses, eccentricity, surface-to-volume ratio, LoG uniformity (σ = 3.5), and LoG skewness (σ = 0.5) were ultimately identified as predictive of tumor DT (Table 2).

The results of subgroup analysis according to tumor growth pattern are presented in Table 3 and Table S3. Majority of patients had tumors with a GP I ($n$ = 41, 78.8%), and the selected radiomic features for predicting tumor DT from GEE analysis were similar to those for total subjects: surface-to-volume ratio, contrast, LoG uniformity (σ = 3.5), and LoG skewness (σ = 0.5) (Table S3). However, in the GP II group ($n$ = 11, 21.2%), the final selected radiomic features for tumor DT prediction were different: roundness factor, solidity, max3D diameter, energy, max probability, intensity variability, LoG kurtosis (σ = 0.5), and fractal signature dissimilarity (Table 3, all *P*-value <0.01). After analyzing the data using multiple GEEs with backward stepwise variable selection, solidity, energy, and busyness were found to be predictive of DT in the GP II group (Table 3).

### Comparison of prediction models

The results of Spearman's correlation analysis of three prediction models are presented in Fig 3. The Spearman correlation coefficients between the observed and predicted DTs were 0.556, 0.606, and 0.887 in total subjects, GP I, and GP II, respectively.

### Survival outcomes

See Appendix S2 and Figure S1.

## Discussion

In this study, we investigated the utility of margin-related radiomic features to predict the tumor DT of lung ADC. Margin-related radiomic characteristics used in this study comprised 76 of 94 total CT radiomic features of three

 © 2020 The Authors. *Thoracic Cancer* published by China Lung Oncology Group and John Wiley & Sons Australia, Ltd. 

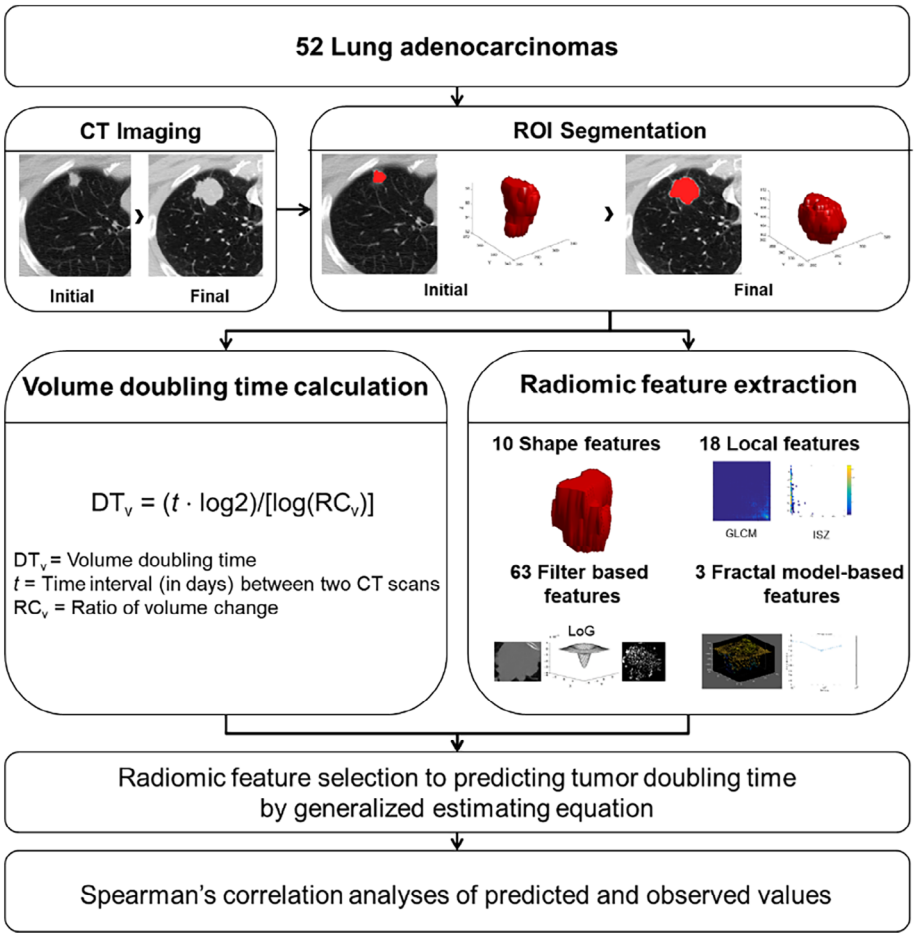


**Figure 2** Development of a tumor DT prediction model based on radiomic characteristics.

main types: 10 shape features, 63 filter-based features (LoG filter), and three fractal model-based features. Shape features describe the three-dimensional size and shape of the tumor region. Filter-based features are composed of histogram-based features of the Laplacian of Gaussian. The Laplacian of an image brings out areas of rapid intensity change and is typically used for edge detection. A Gaussian filter is applied prior to the Laplacian to smooth the image and reduce noise. Scale of texture in LoG (fine to coarse) was specified by modifying the Gaussian radius parameter (from 0.5 to 3.5 in 0.5 voxel increments). Histogram-based features for LoG (mean, maximum, median, minimum, entropy, uniformity, standard deviation, skewness, and kurtosis) were also investigated. Fractal model-based features are composed of a fractal dimension (box-counting), lacunarity, and fractal signature dissimilarity. They describe the heterogeneity of the tumor margin or shape (Appendix S1).[27–30]

Using these features, we found two distinct tumor growth patterns that had specific margin-related radiomic features that were predictive of tumor DT. Our major findings were: (i) for all ADCs, the combination of eccentricity, surface-to-volume ratio, LoG uniformity ($\sigma$ = 3.5), and LoG skewness ($\sigma$ = 0.5) had predictive ability for tumor DT; (ii) the majority of subjects were assigned to the GP I group ($n$ = 41) because they had gradually growing tumors without a temporary decrease in tumor volume, and the finally selected radiomic features for predicting tumor DT in this group were similar to those found for total subjects, namely surface-to-volume ratio, contrast, LoG uniformity ($\sigma$ = 3.5), and LoG skewness ($\sigma$ = 0.5). The only difference between radiomic features predictive of total DT in all subjects versus the GP I group was eccentricity, which was predictive for total subjects. Eccentricity is a measure of how close a shape is to an ellipse on the 2D image; thus, this feature may reflect an increase in tumor margin irregularity in accordance with tumor evolution. We also performed a calibration test using Spearman's correlation analysis by comparing predicted values from the prediction models and observed values. The Spearman correlation coefficients for the observed and predicted DT values were high: 0.606 and

 © 2020 The Authors. *Thoracic Cancer* published by China Lung Oncology Group and John Wiley & Sons Australia, Ltd.

**Table 1** Demographics and tumor characteristics of patients with lung adenocarcinoma

| | Total ($n$ = 52) | GP I ($n$ = 41) | GP II ($n$ = 11) |
|---|---|---|---|
| Sex | | | |
| Male | 26 (50) | 22 (53.7) | 4 (36.4) |
| Female | 26 (50) | 19 (46.3) | 7 (63.6) |
| Age (mean ± SD) (years) | 60.1 ± 18.6 | 59.8 ± 18.6 | 61.2 ± 18 |
| Smoking status | | | |
| Current smoker | 4 (7.7) | 3 (7.3) | 1 (9.1) |
| Ex-smoker | 14 (26.9) | 11 (26.8) | 3 (27.3) |
| Non-smoker | 34 (65.4) | 27 (65.9) | 7 (63.6) |
| Initial tumor size (mean ± SD) (cm) | 2.2 ± 1.7 | 2.4 ± 1.7 | 1.5 ± 1.7 |
| Initial tumor volume (mean ± SD) (voxels) | 5511.9 ± 28 772.9 | 6764.7 ± 28 772.9 | 842.7 ± 28 772 |
| Tumor volume doubling time (mean ± SD) (days) | 1159 ± 2015 | 888 ± 20 | 2171 ± 2015 |
| UICC stage | | | |
| I | 42 (80.8) | 31 (75.6) | 11 (100) |
| II | 4 (7.7) | 4 (9.8) | 0 (0) |
| III | 6 (11.5) | 6 (14.6) | 0 (0) |
| Operation type | | | |
| Wedge resection | 18 (34.6) | 11 (26.8) | 7 (63.6) |
| Lobectomy | 34 (65.4) | 30 (73.2) | 4 (36.4) |
| Pneumonectomy | 0 (0) | 0 (0) | 0 (0) |
| Histologic grade | | | |
| Low | 12 (23.1) | 10 (24.4) | 2 (18.2) |
| Intermediate | 32 (61.5) | 23 (56.1) | 9 (81.8) |
| High | 6 (11.5) | 6 (14.6) | 0 (0) |
| AIS | 1 (1.9) | 1 (2.4) | 0 (0) |
| Unknown | 1 (1.9) | 1 (2.4) | 0 (0) |
| Predominant subtype | | | |
| Lepidic | 8 (15.4) | 7 (17.1) | 1 (9.1) |
| Acinar | 32 (61.5) | 24 (58.5) | 8 (72.7) |
| Papillary | 4 (7.7) | 3 (7.3) | 1 (9.1) |
| Micropapillary | 0 (0) | 0 (0) | 0 (0) |
| Solid | 5 (9.6) | 4 (9.8) | 1 (9.1) |
| Variant | 3 (5.8) | 3 (7.3) | 0 (0) |

Unless otherwise indicated, data are number of patients with percentages in parentheses.

AIS, adenocarcinoma in situ; GP, growth pattern; SD, standard deviation; UICC, Union for International Cancer Control.

**Table 2** Selected radiomic features for predicting tumor doubling time from generalized estimating equations in all lung adenocarcinomas

| | Radiomic features | Univariate | | | Multiple | | |
|---|---|---|---|---|---|---|---|
| | | Coefficient[†] | SE | $P$-value | Coefficient[†] | SE | $P$-value |
| Shape features | **Eccentricity** | 1.201 | 0.5929 | 0.04289 | 0.7222 | 0.4147 | 0.0816 |
| | **Surface-to-volume ratio** | −0.7881 | 0.4671 | 0.09154 | −1.0237 | 0.3834 | 0.0076 |
| Local features (texture-based) | Variance (GLCM) | −0.00002794 | 0.00001113 | 0.01204 | | | |
| | Busyness (NGTDM) | −1.074 | 0.5245 | 0.04057 | | | |
| Filter-based features | LoG mean (σ = 0.5) | 0.0003892 | 0.000176 | 0.02699 | | | |
| | LoG maximum (σ = 1) | 0.003213 | 0.00118 | 0.006463 | | | |
| | LoG uniformity (σ = 3) | −6.375 | 1.773 | 0.0003247 | | | |
| | **LoG uniformity (σ = 3.5)** | −4.079 | 1.1 | 0.0002087 | −2.2418 | 1.0026 | 0.0254 |
| | **LoG skewness (σ = 0.5)** | −0.5456 | 0.1797 | 0.002397 | −0.4953 | 0.1768 | 0.0051 |
| | LoG kurtosis (σ = 1) | −0.3122 | 0.1191 | 0.008781 | | | |

GLCM, gray level co-occurrence matrix-based features; LoG, Laplacian of Gaussian Features in bold are those that were selected from the multiple generalized estimating equation; NGTDM, neighborhood gray tone difference matrix-based features; SE, standard error.

[†]Coefficient estimated by generalized estimating equation.

 © 2020 The Authors. *Thoracic Cancer* published by China Lung Oncology Group and John Wiley & Sons Australia, Ltd. 

**Table 3** Selected radiomic features for predicting tumor doubling time from generalized estimating equations in growth pattern II lung adenocarcinomas

| | Radiomic features | Simple | | | Multiple‡ | | |
|---|---|---|---|---|---|---|---|
| | | Coefficient† | SE | *P*-value | Coefficient† | SE | *P*-value |
| Shape features | **Roundness factor** | −3.06 | 1.15 | 0.00786 | | | |
| | **Solidity‡** | −4.58 | 1.53 | 0.00279 | −11.119 | 1.65 | 1.60E-11 |
| | Surface area | 0.000956 | 0.000406 | 0.0187 | | | |
| | **Max3D diameter** | 0.0527 | 0.0168 | 0.00176 | | | |
| Local features (texture-based) | Auto correlation (GLCM) | −0.0000321 | 0.0000147 | 0.0295 | | | |
| | Cluster tendency (GLCM) | −0.00000812 | 0.00000369 | 0.0277 | | | |
| | Dissimilarity (GLCM) | −0.0428 | 0.0238 | 0.0721 | | | |
| | Entropy (GLCM) | 0.285 | 0.149 | 0.0552 | | | |
| | **Energy (GLCM)‡** | −243 | 86.3 | 0.0048 | 297.929 | 62.323 | 1.70E-06 |
| | Homogeneity (GLCM) | 16.4 | 5.6 | 0.00345 | | | |
| | **Max probability (GLCM)** | −100 | 34.5 | 0.0037 | | | |
| | Variance (GLCM) | −0.0000329 | 0.0000148 | 0.0262 | | | |
| | **Intensity variability (ISZM)** | 0.0156 | 0.00479 | 0.00111 | | | |
| | Size zone variability (ISZM) | 0.0721 | 0.0283 | 0.0108 | | | |
| | Contrast (NGTDM) | −1.68 | 0.858 | 0.0504 | | | |
| | Busyness (NGTDM)‡ | | | | −54.661 | 15.476 | 0.00041 |
| Filter-based features | LoG entropy (σ = 1.5) | 0.403 | 0.232 | 0.0829 | | | |
| | LoG entropy (σ = 2) | 0.505 | 0.298 | 0.0906 | | | |
| | LoG uniformity (σ = 1.5) | −38.5 | 18.2 | 0.0351 | | | |
| | LoG uniformity (σ = 2) | −29.5 | 13.6 | 0.0303 | | | |
| | LoG uniformity (σ = 3) | −7.46 | 3.23 | 0.0208 | | | |
| | LoG uniformity (σ = 3.5) | −4.53 | 2.28 | 0.0465 | | | |
| | **LoG kurtosis (σ = 0.5)** | 0.835 | 0.257 | 0.00113 | | | |
| Fractal model-based features | Lacunarity | 0.336 | 0.146 | 0.0213 | | | |
| | **Fractal signature dissimilarity** | −0.536 | 0.187 | 0.00409 | | | |

†Coefficient estimated by generalized estimating equation.

‡Variables were selected using a backward stepwise variable selection method.

Variables in bold are those that had clinical significance without redundancy within the radiomic information as well as a *P*-value < 0.01 after multiple generalized estimating equation analysis.

GLCM, gray level co-occurrence matrix-based features; ISZM, intensity size zone matrix-based features; LoG, Laplacian of Gaussian; NGTDM, neighborhood gray tone difference matrix-based features; SE, standard error.

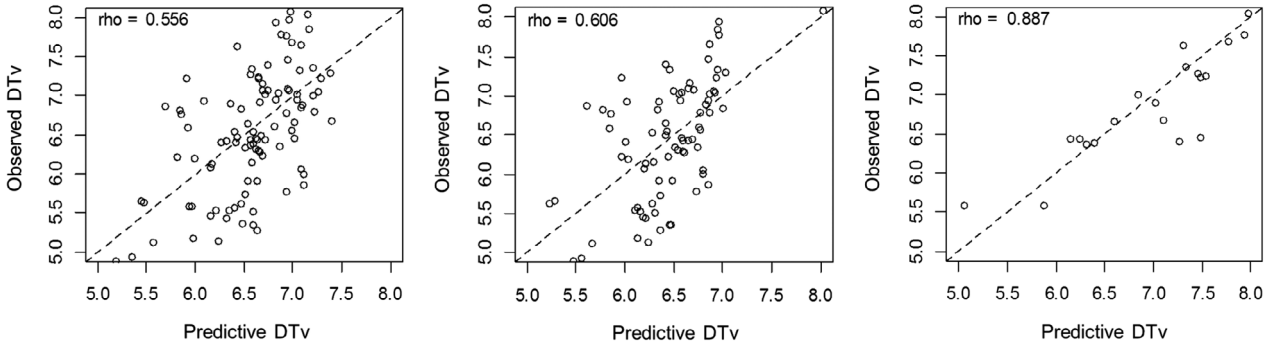


**Figure 3** Spearman's correlation analysis results for predicted values and observed values to compare prediction models. Spearman correlation coefficients for observed versus predicted DTs were 0.556, 0.606, and 0.887 for (**a**) total subjects; (**b**) growth pattern I; and (**c**) growth pattern II groups, respectively.

 © 2020 The Authors. *Thoracic Cancer* published by China Lung Oncology Group and John Wiley & Sons Australia, Ltd.

0.887 for groups GP I and GP II, respectively. Based on these results, it appears that margin- or shape-related radiomic features extracted from the initial CT scan might reflect the growth kinetics of lung ADCs.

Several previous studies have investigated the microenvironment of the tumor perimeter.[31–33] Tumor-infiltrating lymphocytes, often found in the stroma around the tumor, play an important role in immunosurveillance and tumor rejection.[31] In lung cancers, the density of stromal macrophage infiltration has been shown to be associated with tumor stage and the likelihood of metastasis.[32] Tripathi *et al.* found that neoplastic infiltration of malignant nodules distorted the neighboring tissue.[33] Thus, histopathological tumor margin or peritumoral characteristics, which may contribute to the imaging appearance of a tumor, could reflect changes to the microenvironment based on interactions between the tumor and surrounding parenchyma. We therefore hypothesized that margin-related radiomic features might predict tumor behavior and/or growth of lung ADCs.

Lung ADCs may grow due to multistep progression from atypical adenomatous hyperplasia (AAH) through AIS or MIA to ADC.[6, 34] It is generally accepted that a GGO nodule increases in size, then a solid portion appears, and finally the solid portion increases in extent.[34] Kakinuma *et al.*[22] however, found that malignant GGO nodules did not always increase in size or attenuation but sometimes decreased in size. Interestingly, in our study, during the follow-up period prior to surgical resection, a temporary decrease in tumor volume on serial CT scans occurred in 11 (21.2%) cases of tumors with a GGO component. This temporary decrease in tumor volume, which corresponds to a negative DT, is likely due to tumor volume shrinkage caused by alveolar collapse and central fibrosis with tumor progression.[21, 22] Honda *et al.*[35] and Koike *et al.*[20] determined the volumetric DTs of lung cancers and reported negative DTs for five of 40 (12.5%) and 11 of 70 (15.7%) adenocarcinomas, respectively, similar to our observations. Interestingly, in the 11 tumors with a negative DT (GP II group), the final radiomic features selected for DT prediction were quite different from those of the total and GP I group. They were solidity, energy, and busyness (Table 3), with solidity being the most significant feature. This finding is meaningful because a temporary decrease in tumor volume (GP II) tends to occur in some adenocarcinomas with a predominant GGO (negative solidity) that becomes denser and smaller due to alveolar collapse or central fibrosis.[21, 22] This explains why solidity on the initial CT scan is relevant to DT prediction in GP II tumors. Based on our findings, if a lung ADC has a prominent GGO portion and a temporary negative DT on serial CT, DT prediction modeling should be performed separately according to growth pattern.

For radiomic analysis, we focused more on margin-related features than intratumoral features. Shape- or margin-based classification of lung tumors is different from textural analysis. Nonshape features such as textural- and intensity-based features may be more affected by intensity and scanner variability.[18] In other words, different CT scanners and scanning parameters such as slice thickness and reconstruction algorithms could affect the resulting textural features.[36] By contrast, margin-related features tend to be less sensitive to differences in image intensity and scanner platforms and potentially more predictive of lesion diagnosis than texture features. Our use of margin-related radiometric features is one of the strengths of our study.

However, reproducibility of margin-related radiomic features might be a critical issue because all radiomic features were extracted from manually derived ROIs. For this reason, two readers independently performed manual segmentation of ROIs on axial CT images, and we evaluated the stability of various radiomic features by calculating ICC as a measure of interobserver reliability. Most radiomic features showed very good or excellent reproducibility, and the mean ICC value was 0.91, indicating excellent agreement. The exception was kurtosis-related filter-based features, which showed a relatively lower level of agreement (ICC = 0.62–0.90) (Table S2). The reason for the lower ICC values of kurtosis-related filter-based features is unclear, and there is no previous research that can shed light on this issue. Further study of this finding is needed in the future.

In the survival analysis, the OS and DFS were slightly better in GP II than those of GP I (Appendix S2 and Figure S1). We assumed that DT was in inverse proportion to the prognosis, thus, GP I with shorter DT (888 days) might have worse prognosis than GP II with longer DT (2171 days). Even though the study population was relatively small to have statistical power, and GP I had some advanced stage cases, these tumor DT might have an effect on survival outcomes.

Our study had several limitations. First, the data were retrospective and limited to 52 patients from a single institution. Furthermore, we only selected tumors that were histologically proven after surgical resection. This might have caused selection bias. Nevertheless, 52 subjects is a reasonable subject size because it is difficult to find patients who have relatively long-term, preoperative, serial follow-up CT scans prior to surgery. This deficiency could be addressed in future work by using a larger patient cohort. Second, we did not perform external validation using an independent population. However, we conducted this study with a calibration test using Spearman's correlation analysis to verify our results. Third, because of differences in subgroup sizes, the generalizability of our findings is

 © 2020 The Authors. *Thoracic Cancer* published by China Lung Oncology Group and John Wiley & Sons Australia, Ltd. 

limited. Finally, a negative DT could result from uncertainties in tumor volume determination. In cases where the tumor volume did not change much, the second volume could be smaller than the initial volume based on absolute numbers, but might be the same or vice versa within the error bars. To avoid calculation errors, we double-checked the DT results and minimized such cases.

In conclusion, we analyzed the associations between margin-related radiomic features and tumor DT and found a relationship between radiomic features and tumor growth rate. This study demonstrates the potential of margin-related radiomic features to capture properties of the tumor microenvironment that in turn reflect tumor growth. These margin-related radiomic features can potentially be used as noninvasive biomarkers to predict tumor DT in lung ADC and inform treatment strategies.

## Acknowledgments

This research was supported by the Korea Health Technology R&D Project through the Korea Health Industry Development Institute (KHIDI), which was funded by the Ministry of Health & Welfare (HI17C0086). In addition, this work was supported by National Research Foundation of Korea (NRF) grants funded by the Korean government (MSIP; Ministry of Science, ICT, & Future Planning) (NRF-2016R1A2B4013046 and NRF-2017M2A2A7A02018568). The sponsors had no role in the study design, data collection and analysis, or manuscript preparation. We would like to thank Sook Lee for performing the experimental work.

## Disclosure

The authors declare that they have no competing interests.

## References

1 MacMahon H, Austin JH, Gamsu G *et al.* Guidelines for management of small pulmonary nodules detected on CT scans: A statement from the Fleischner Society. *Radiology* 2005; **237**: 395–400.
2 Revel MP, Merlin A, Peyrard S *et al.* Software volumetric evaluation of doubling times for differentiating benign versus malignant pulmonary nodules. *Am J Roentgenol* 2006; **187**: 135–42.
3 Winer-Muram HT, Jennings SG, Tarver RD *et al.* Volumetric growth rate of stage I lung cancer prior to treatment: Serial CT scanning. *Radiology* 2002; **223**: 798–805.
4 Min JH, Lee HY, Lee KS *et al.* Stepwise evolution from a focal pure pulmonary ground-glass opacity nodule into an invasive lung adenocarcinoma: An observation for more than 10 years. *Lung Cancer* 2010; **69**: 123–6.
5 Mackintosh JA, Marshall HM, Yang IA, Bowman RV, Fong KM. A retrospective study of volume doubling time in surgically resected non-small cell lung cancer. *Respirology* 2014; **19**: 755–62.
6 Aoki T, Nakata H, Watanabe H *et al.* Evolution of peripheral lung adenocarcinomas: CT findings correlated with histology and tumor doubling time. *Am J Roentgenol* 2000; **174**: 763–8.
7 Heuvelmans MA, Oudkerk M, de Bock GH *et al.* Optimisation of volume-doubling time cutoff for fast-growing lung nodules in CT lung cancer screening reduces false-positive referrals. *Eur Radiol* 2013; **23**: 1836–45.
8 Veronesi G, Maisonneuve P, Bellomi M *et al.* Estimating overdiagnosis in low-dose computed tomography screening for lung cancer: A cohort study. *Ann Intern Med* 2012; **157**: 776–84.
9 Suzuki K, Kusumoto M, Watanabe S, Tsuchiya R, Asamura H. Radiologic classification of small adenocarcinoma of the lung: Radiologic-pathologic correlation and its prognostic impact. *Ann Thorac Surg* 2006; **81**: 413–9.
10 Asamura H, Hishida T, Suzuki K *et al.* Radiographically determined noninvasive adenocarcinoma of the lung: Survival outcomes of Japan Clinical Oncology Group 0201. *J Thorac Cardiovasc Surg* 2013; **146**: 24–30.
11 Lee G, Lee HY, Ko ES, Jeong WK. Radiomics and imaging genomics in precision medicine. *Precis Future Med* 2017; **1**: 10–31.
12 Kumar V, Gu Y, Basu S *et al.* Radiomics: The process and the challenges. *Magn Reson Imaging* 2012; **30**: 1234–48.
13 Lambin P, Rios-Velazquez E, Leijenaar R *et al.* Radiomics: Extracting more information from medical images using advanced feature analysis. *Eur J Cancer* 2012; **48**: 441–6.
14 Braman NM, Etesami M, Prasanna P *et al.* Intratumoral and peritumoral radiomics for the pretreatment prediction of pathological complete response to neoadjuvant chemotherapy based on breast DCE-MRI. *Breast Cancer Res* 2017; **19**: 57.
15 Dilger SK, Uthoff J, Judisch A *et al.* Improved pulmonary nodule classification utilizing quantitative lung parenchyma features. *J Med Imaging (Bellingham)* 2015; **2**: 041004.
16 Lemee JM, Clavreul A, Menei P. Intratumoral heterogeneity in glioblastoma: don't forget the peritumoral brain zone. *Neuro Oncol* 2015; **17**: 1322–32.
17 Wu J, Li B, Sun X *et al.* Heterogeneous enhancement patterns of tumor-adjacent parenchyma at MR imaging are associated with dysregulated signaling pathways and poor survival in breast cancer. *Radiology* 2017; **285**: 401–13.
18 Alilou M, Beig N, Orooji M *et al.* An integrated segmentation and shape-based classification scheme for distinguishing adenocarcinomas from granulomas on lung CT. *Med Phys* 2017; **44**: 3556–69.
19 Travis WD, Brambilla E, Noguchi M *et al.* International association for the study of lung cancer/american thoracic society/european respiratory society international

 © 2020 The Authors. *Thoracic Cancer* published by China Lung Oncology Group and John Wiley & Sons Australia, Ltd.

multidisciplinary classification of lung adenocarcinoma. *J Thorac Oncol* 2011; **6**: 244–85.
20 Koike W, Iwano S, Matsuo K, Kitano M, Kawakami K, Naganawa S. Doubling time calculations for lung cancer by three-dimensional computer-aided volumetry: Effects of inter-observer differences and nodule characteristics. *J Med Imaging Radiat Oncol* 2014; **58**: 82–8.
21 Terasaki H, Kato S, Matsuno Y *et al.* Lung adenocarcinoma, mixed subtype: Histopathologic basis for high-resolution computed tomography findings. *J Thorac Imaging* 2011; **26**: 74–81.
22 Kakinuma R, Ohmatsu H, Kaneko M *et al.* Progression of focal pure ground-glass opacity detected by low-dose helical computed tomography screening for lung cancer. *J Comput Assist Tomogr* 2004; **28**: 17–23.
23 van Griethuysen JJM, Fedorov A, Parmar C *et al.* Computational radiomics system to decode the radiographic phenotype. *Cancer Res* 2017; **77**: e104–e7.
24 Cho HH, Lee G, Lee HY, Park H. Marginal radiomics features as imaging biomarkers for pathological invasion in lung adenocarcinoma. *Eur Radiol* 2020; **30**: 2984–94.
25 Song SH, Park H, Lee G *et al.* Imaging phenotyping using radiomics to predict micropapillary pattern within lung adenocarcinoma. *J Thorac Oncol* 2017; **12**: 624–32.
26 Liu Y, Zhang Y, Cheng R *et al.* Radiomics analysis of apparent diffusion coefficient in cervical cancer: A preliminary study on histological grade evaluation. *J Magn Reson Imaging* 2019; **49**: 280–90.
27 Kido S, Kuriyama K, Higashiyama M, Kasugai T, Kuroda C. Fractal analysis of internal and peripheral textures of small peripheral bronchogenic carcinomas in thin-section computed tomography: Comparison of bronchioloalveolar cell carcinomas with nonbronchioloalveolar cell carcinomas. *J Comput Assist Tomogr* 2003; **27**: 56–61.
28 Lennon FE, Cianci GC, Cipriani NA *et al.* Lung cancer-a fractal viewpoint. *Nat Rev Clin Oncol* 2015; **12**: 664–75.
29 Paskas MP, Reljin IS, Reljin BD. Multifractal framework based on blanket method. *ScientificWorldJournal* 2014; **2014**: 894546.
30 Wang C, Subashi E, Yin FF, Chang Z. Dynamic fractal signature dissimilarity analysis for therapeutic response assessment using dynamic contrast-enhanced MRI. *Med Phys* 2016; **43**: 1335–47.
31 Badalamenti G, Fanale D, Incorvaia L *et al.* Role of tumor-infiltrating lymphocytes in patients with solid tumors: Can a drop dig a stone? *Cell Immunol* 2019; **343**: 103753.
32 Banat GA, Tretyn A, Pullamsetti SS *et al.* Immune and inflammatory cell composition of human lung cancer stroma. *PLOS One* 2015; **10**: e0139073.
33 Tripathi S, Zhen X. Differentiation of benign and malignant solitary pulmonary nodule: Literature review. *Adv Lung Cancer* 2015; **04**: 8.
34 Takashima S, Maruyama Y, Hasegawa M *et al.* CT findings and progression of small peripheral lung neoplasms having a replacement growth pattern. *AJR Am J Roentgenol* 2003; **180**: 817–26.
35 Honda O, Johkoh T, Sekiguchi J *et al.* Doubling time of lung cancer determined using three-dimensional volumetric software: Comparison of squamous cell carcinoma and adenocarcinoma. *Lung Cancer* 2009; **66**: 211–7.
36 Zhao B, Tan Y, Tsai WY, Schwartz LH, Lu L. Exploring variability in CT characterization of tumors: A preliminary phantom study. *Transl Oncol* 2014; **7**: 88–93.

## Supporting Information

Additional Supporting Informationmay be found in the online version of this article at the publisher's website:

**Appendix**: **S1** Supporting Information

 © 2020 The Authors. *Thoracic Cancer* published by China Lung Oncology Group and John Wiley & Sons Australia, Ltd. 